

AD-766 234

PROPERTIES OF UNIFORM COHERENT FREQUENCY-
JUMP WAVEFORMS

A. F. Culmone

Massachusetts Institute of Technology
Lexington, Massachusetts

April 1973

DISTRIBUTED BY:

NTIS

National Technical Information Service
U. S. DEPARTMENT OF COMMERCE
5285 Port Royal Road, Springfield Va. 22151

ESD-TR 73-230

CALSPAN NO. TD-5048-S-7
APRIL 1973

AD 766234

TECHNICAL NOTE
PROPERTIES OF UNIFORM COHERENT FREQUENCY-JUMP WAVEFORMS

A.F. Culmone

DDC
SEP 5
1973

Prepared by
CALSPAN CORPORATION
(FORMERLY CORNELL AERONAUTICAL LABORATORY, INC.)

Reproduced by
**NATIONAL TECHNICAL
INFORMATION SERVICE**
U S Department of Commerce
Springfield VA 22151

Prepared For
**MASSACHUSETTS INSTITUTE OF TECHNOLOGY
LINCOLN LABORATORY**
FOR THE OFFICE OF THE CHIEF OF RESEARCH AND
DEVELOPMENT, DEPARTMENT OF THE ARMY

DISTRIBUTION STATEMENT A
Approved for public release
Distribution Unlimited

43

**APPROVED FOR PUBLIC RELEASE;
DISTRIBUTION UNLIMITED.**

100		
101		
102		
103		
104		
105		
106		
107		
108		
109		
110		
111		
112		
113		
114		
115		
116		
117		
118		
119		
120		
121		
122		
123		
124		
125		
126		
127		
128		
129		
130		
131		
132		
133		
134		
135		
136		
137		
138		
139		
140		
141		
142		
143		
144		
145		
146		
147		
148		
149		
150		
151		
152		
153		
154		
155		
156		
157		
158		
159		
160		
161		
162		
163		
164		
165		
166		
167		
168		
169		
170		
171		
172		
173		
174		
175		
176		
177		
178		
179		
180		
181		
182		
183		
184		
185		
186		
187		
188		
189		
190		
191		
192		
193		
194		
195		
196		
197		
198		
199		
200		

Unclassified

Security Classification

DOCUMENT CONTROL DATA - R & D		
<i>(Security classification of title, body of abstract and indexing annotation must be entered when the overall report is classified)</i>		
1. ORIGINATING ACTIVITY (Corporate author) Calspan Corporation; Buffalo, New York 14221 under Purchase Order No. B-248 to M.I.T., Lincoln Laboratory		2a. REPORT SECURITY CLASSIFICATION UNCLASSIFIED
		2b. GROUP
3. REPORT TITLE PROPERTIES OF UNIFORM COHERENT FREQUENCY-JUMP WAVEFORMS		
4. DESCRIPTIVE NOTES (Type of report and inclusive dates) Technical Note		
5. AUTHOR(S) (First name, middle initial, last name) A. F. Culmone		
6. REPORT DATE April 1973	7a. TOTAL NO. OF PAGES 43	7b. NO. OF REFS None
6a. CONTRACT OR GRANT NO. F19628-73-C-0002	8a. ORIGINATOR'S REPORT NUMBER(S) Calspan Report No. TD-5048-S-7	
b. PROJECT NO. 7X263304D215	9b. OTHER REPORT NO(S) (Any other numbers that may be assigned this report) ESD-TR-73-230	
d. Purchase Order No. B-248		
10. DISTRIBUTION STATEMENT Approved for public release; distribution unlimited.		
11. SUPPLEMENTARY NOTES None	12. SPONSORING MILITARY ACTIVITY Office of the Chief of Research and Development, Department of the Army	
13. ABSTRACT A frequency-jump burst waveform is a sequence of pulses each having the same complex envelope but a different center frequency. When transmitted and received coherently, such a sequence has a range resolution which corresponds to the total bandwidth of the waveform, which may be much greater than that of the receiver IF and video circuitry. Frequency-jump burst waveforms which consist of linear FM pulses uniformly spaced in time and center frequency are considered. Their resolution and ambiguity properties are derived and certain error sources analyzed. In particular, waveforms which are implementable in TRADEX are proposed and evaluated.		

DD FORM 1 NOV 65 1473

Unclassified

Security Classification

Unclassified

Security Classification

14. KEY WORDS	LINK A		LINK B		LINK C	
	ROLE	WT	ROLE	WT	ROLE	WT
coherent pulse trains						
frequency-jump waveforms						
synthetic widebandwidth						
ambiguity function structure						

Unclassified

Security Classification

11

CALSPAN NO. TD-5048-S-7
APRIL 1973

PROPERTIES OF UNIFORM COHERENT FREQUENCY-JUMP WAVEFORMS

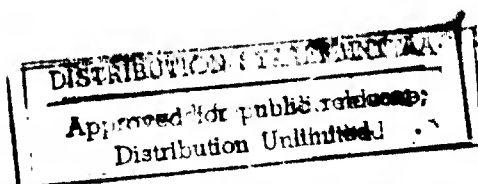
A.F. Culmone

Prepared by
CALSPAN CORPORATION
(FORMERLY CORNELL AERONAUTICAL LABORATORY, INC.)

FOR
MASSACHUSETTS INSTITUTE OF TECHNOLOGY
LINCOLN LABORATORY
FOR THE OFFICE OF THE CHIEF OF RESEARCH AND
DEVELOPMENT, DEPARTMENT OF THE ARMY

UNDER
PURCHASE ORDER NO. B-248
PRIME CONTRACT NO. F19628-73-C-0002
PROJECT NO. 7X263304D215

APPROVED FOR PUBLIC RELEASE;
DISTRIBUTION UNLIMITED.



PROPERTIES OF UNIFORM COHERENT FREQUENCY-JUMP WAVEFORMS

Abstract

A frequency-jump burst waveform is a sequence of pulses each having the same complex envelope but a different center frequency. When transmitted and received coherently, such a sequence has a range resolution which corresponds to the total bandwidth of the waveform, which may be much greater than that of the receiver IF and video circuitry. Frequency-jump burst waveforms which consist of linear FM pulses uniformly spaced in time and center frequency are considered. Their resolution and ambiguity properties are derived and certain error sources analyzed. In particular, waveforms which are implementable in TRADEX are proposed and evaluated.

Accepted for the Air Force
Joseph J. Whelan, USAF
Acting Chief, Lincoln Laboratory Liaison Office

CONTENTS

	<u>Page</u>
ABSTRACT	iii
LIST OF FIGURES	vi
LIST OF TABLES	vi
1.0 INTRODUCTION	1
2.0 WAVEFORM PROPERTIES	3
2.1 Resolution Properties	3
2.2 Uniform Coherent Pulse Trains	4
2.3 Waveform Autocorrelation Function	7
3.0 WAVEFORM DESIGN	9
3.1 Ambiguity Function Structure	9
3.2 Single-Pulse Sidelobe Suppression	12
3.3 Sidelobe Suppression for Coherent Pulse Trains	14
3.4 Near-Range Ambiguity Characteristics	16
3.5 Far-Range Ambiguity Characteristics	17
4.0 SYSTEMS CONSIDERATIONS	19
4.1 Quantization Errors	19
4.2 Sampling Errors	22
5.0 SUMMARY	24
6.0 APPENDICES	25
6.1 Properties of the Return Signal	25
6.2 Analysis of Quantization Errors	27
6.3 Analysis of Sampling Errors	31
6.4 Coherent Frequency-Jump Burst Waveforms for TRADEX	33

LIST OF FIGURES

		<u>Page</u>
2.1	Sum of Phase Terms of $\phi(T)$ at a Particular $T(\Theta)$. . .	6
2.2	Sum of Phase Terms of $\phi(T)$ versus $T(\Theta)$	7
3.1	Frequency Jump Burst Waveform Ambiguity Function	10
3.2	Factors of the Ambiguity Function	11
3.3	Hamming Weighting	13
3.4	Origin of Far-Range Ambiguities	17
6.1	Normalized Mean Square Error Due to Amplitude Quantization	29
6.2	Normalized Mean Square Error Due to Phase Quantization	30
6.3	Spectrum of Signal Sampled at $1/2$ Nyquist Rate . . .	31
6.4	Interpretation of Quantities in Table 6.1	34
6.5	Constant-Velocity Profiles for Waveform 1	35
6.6	Constant-Velocity Profiles for Waveform 3	36

LIST OF TABLES

6.1	Properties of Candidate Waveforms for TRADEX . . .	34
-----	--	----

1.0 INTRODUCTION

In certain applications there is a need for radar waveforms having very fine range and/or velocity resolution. Many waveforms can be designed to provide the required resolution, but not all are realizable since the hardware performance of existing radar systems places constraints upon the implementation of fine resolution waveforms. Therefore, it is within such constraints that practical waveform design must be carried out.

Generally, high resolution waveforms have been mainly limited by the time-bandwidth (TW) product permitted by the hardware technology. The waveform design process can then be loosely described as one whose objective is to achieve sufficiently large values of T and W to satisfy requirements for velocity and range resolution respectively while remaining constrained to an achievable TW product.

A severe constraint on any radar system is the bandwidth of the circuitry. Large bandwidths required for fine range resolution may not be practical. An alternative to a wideband system is a narrowband system with the capability of shifting its pass-band sufficiently to cover the required bandwidth. By transmitting a coherent sequence of narrow-band pulses with frequency shifts between pulses, a range resolution capability similar to that for a single pulse with the same overall bandwidth can be achieved.

The use of coherent sequences of pulses is a straightforward technique for controlling the TW product of a waveform. Such coherent sequences are studied in this report. In particular, attention is given to coherent pulse trains having uniform time and frequency spacings. After giving a qualitative description of some pertinent waveform properties in Section 2.0, the quantitative information that is pre-requisite to choosing satisfactory waveforms is provided in Section 3.0. Further, certain system considerations which are critical to the implementation of these waveforms are analyzed in Section 4.0 for the purpose of establishing

operating requirements. A summary of the salient features of this study is presented in Section 5.0. The Appendices of Section 6.0 contain relevant mathematical developments and a summary of properties of frequency-jump burst waveforms implementable in TRADEX.

2.0 WAVEFORM PROPERTIES

In this section, a qualitative discussion of some fundamental signal properties is given in the framework of the design of fine resolution coherent waveforms. In order to preserve some generality, the concepts of range resolution and velocity resolution are replaced with the equivalent notions of time resolution and frequency resolution. When these concepts are applied to the problem of measuring range and velocity, the relationships between time and range and between frequency and velocity are established on a physical basis.

2.1 Resolution Properties

The time resolution capability of a signal can be quantitatively expressed in several ways. A useful measure that has practical importance is based upon the autocorrelation, $\phi(t)$, of the signal, $s(t)$.

$$\phi(t) = \int_{-\infty}^{\infty} s(\tau) s^*(\tau - t) d\tau \quad (2.1)$$

The utility of (2.1) is due, in part, to the fact that for most radar systems the received signal is passed through a filter having nearly the same time response as the signal. Thus, the output of the radar receiver is $\phi(t)$.

It is easy to show, using the Schwarz inequality, that $\phi(t)$ achieves its greatest magnitude when $t=0$. This property enables one of the correlating signals to be located in time when the time reference of the other is known. How well the time location can be measured will certainly depend upon the sharpness of the peak of $\phi(t)$ about $t = 0$. The radius of curvature of the peak may be used as a measure of the time resolution capability of the signal. The radius of curvature of $\phi(t)$ at $t = 0$, which is the reciprocal of the second derivative of $\phi(t)$ evaluated at $t = 0$, is

$$\left. \frac{d^2 \phi(t)}{dt^2} \right|_{t=0} = \int_{-\infty}^{\infty} s(\tau) s^{*''}(\tau) d\tau = \int_{-\infty}^{\infty} |s'(\tau)|^2 d\tau = \frac{-1}{2\pi} \int_{-\infty}^{\infty} \omega^2 |S(\omega)|^2 d\omega \quad (2.2)$$

The second integral is obtained using integration by parts. The third integral follows from Parseval's formula where $S(\omega)$ is the Fourier transform for $\Delta(t)$. The last integral in (2.2) is recognized as the mean-squared (MS) bandwidth of $\Delta(t)$ ¹. The immediate conclusion is that for the measure postulated, the time resolution capability of a signal increases directly as the MS bandwidth.

The absolute bandwidth of a strictly bandlimited signal is sometimes used to give a measure of the time resolution property of a signal. In general, this bandwidth does not imply anything about the resolving property of signals except when dealing with particular classes of signals. The MS bandwidth is often much smaller than the square of the absolute bandwidth. One reason for the significance of the MS bandwidth as a measure of resolution capability is that it is also a measure of the spectral distribution of signal energy, as can be observed from the last integral of (2.2). If a significant portion of the signal energy is concentrated at extreme frequencies, the MS bandwidth will be relatively large among the class of signals with the same absolute bandwidth. The resolving capability of the signal will then be relatively high.

The duality of the Fourier transform pair enables one to make a similar argument for frequency resolution. Thus, the frequency resolution increases directly as the mean-squared time duration,

$$\int_{-\infty}^{\infty} t^2 |\Delta(t)|^2 dt.$$

2.2 Uniform Coherent Pulse Trains

Based upon a reasonable measure of resolution capability it has been shown that the mean squared bandwidth and time duration of a signal are parameters of fundamental importance. The mechanism by which uniform coherent pulse trains can be used to achieve fine resolution is now considered. First, a few preliminaries will be set down.

1. $\Delta(t)$ is a unit energy signal i. e.,

$$\int_{-\infty}^{\infty} |\Delta(t)|^2 dt = 1$$

Throughout this report, the only signals that will be considered are linear FM pulses. A representation of a linear FM pulse is

$$\omega(t) = \begin{cases} \frac{1}{\sqrt{T}} e^{j\pi \frac{B}{T} t^2} & |t| \leq \frac{T}{2} \\ 0 & |t| \geq \frac{T}{2} \end{cases},$$

where B is the instantaneous bandwidth in Hertz and T is the time duration in seconds.

Let

$$\omega_k(t) = \omega(t - k\Delta_t) e^{j2\pi k\Delta_f t} \quad (2.3)$$

be a time-delayed and frequency-shifted representation of the basic pulse $w(t)$ with frequency shift $k\Delta_f$ and time shift $k\Delta_t$. A coherent train of N pulses can then be written as

$$s(t) = \frac{1}{N} \sum_{k=-\frac{(N-1)}{2}}^{\frac{(N-1)}{2}} \omega_k(t) \quad (2.4)$$

where, for convenience, N is assumed to be odd. The pulse train (2.4) is a sequence of pulses uniformly spaced in time and frequency. The time spacing is Δ_t and the frequency spacing is Δ_f . The restriction to uniform time and frequency spacings is made here for three reasons. First of all, the TRADEX frequency-jump burst waveform is initially planned to be uniform in this manner. Second, this is the case which is most easily understood, since it is in many ways a discrete analog of the ordinary linear FM waveform. Third, it is easily analyzed since the ambiguity function (see Section 2.3) can be written in closed form. A qualitative examination of the time resolving properties of $s(t)$ follows.

Assume that $s(t)$ has been time shifted an amount τ to produce $s(t - \tau)$.

$$s(t - \tau) = \frac{1}{N} \sum_{k=-\frac{(N-1)}{2}}^{\frac{(N-1)}{2}} \omega_k(t - \tau) = \frac{1}{N} \sum_{k=-\frac{(N-1)}{2}}^{\frac{(N-1)}{2}} \omega(t - \tau - k\Delta_t) e^{j2\pi k\Delta_f t} \cdot e^{-j2\pi k\Delta_f \tau} \quad (2.5)$$

The delay, τ , is manifest through the phase factor $e^{-j2\pi k\Delta_f\tau}$. When the shifted signal $s(t-\tau)$ is correlated with the reference signal $s(t)$, as in (2.1), it follows from (2.1), (2.4), and (2.5) that

$$\phi(\tau) = \int_{-\infty}^{\infty} s(t) s^*(t-\tau) dt = \frac{1}{N} \sum_{k=-\frac{(N-1)}{2}}^{\frac{(N-1)}{2}} e^{j2\pi k\Delta_f\tau} \int_{-\infty}^{\infty} \omega(t-k\Delta_t) \omega^*(t-\tau-k\Delta_t) dt, \quad (2.6)$$

$|\tau| < \Delta_t - \tau$

It has been assumed in arriving at (2.6), that the pulse spacing, Δ_t , is greater than the pulse duration, τ , so that the pulses do not overlap in time. The range of τ is restricted so that adjacent pulses do not correlate.

Comparing the integral in (2.6) with equation (2.1) shows that the integral is the autocorrelation function for the basic pulse and is independent of k . The variation of the integral due to changes in τ will be disregarded compared with the effect of variations in the phase factors $e^{j2\pi k\Delta_f\tau}$, ($k = -\frac{(N-1)}{2}, \dots, \frac{(N-1)}{2}$). Then, (2.6) can be approximated as the sum of equal amplitude phasors, $e^{j2\pi k\Delta_f\tau}$. With this approximation $\phi(\tau)$ is periodic in τ , with period $\tau_p = \frac{1}{\Delta_f}$. This period, which depends on only the interpulse frequency spacing, corresponds to a coarse time-range side-lobe. This will be shown later.

There are additional periodicities in $\phi(\tau)$ that depend upon the number of pulses or, equivalently, the total bandwidth occupied by the N pulses. In (2.6), the interpulse phase is the same for all successive pairs of pulses. Let this phase be $\theta = 2\pi\Delta_f\tau$ and consider the sum of equal amplitude phasors as shown in Figure 2.1.

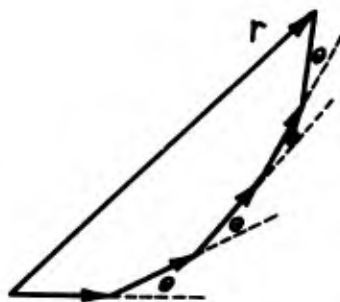


Figure 2.1 SUM OF PHASE TERMS OF $\phi(\tau)$ AT A PARTICULAR τ (θ)

It is easily shown that the locus, as a function of θ , for the tip of the resultant phasor, r , is as it appears in Figure 2.2.

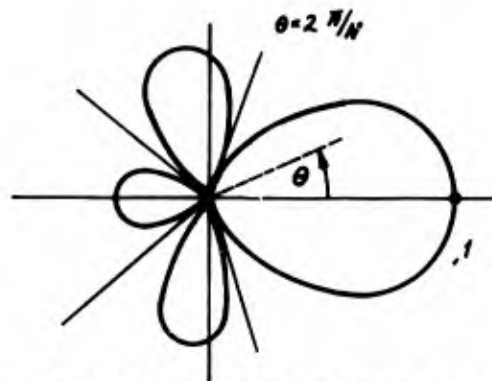


Figure 2.2 SUM OF PHASE TERMS OF $\phi(\tau)$ VERSUS $\tau(\theta)$

The locus in Figure 2.2 gives an approximate representation for the magnitude of $\phi(\tau)$. The locus passes through the origin $N-1$ times, defining a time sidelobe each time. It is easy to see that as the number of pulses increases, the variation of r in Figure 2.1 will be more rapid. This representation graphically establishes the connection between the bandwidth and the time resolving property of $\phi(\tau)$ (recall that θ is a linear function of τ). Again, equivalent properties exist for frequency resolution.

2.3 Waveform Autocorrelation Function

The two dimensional time-frequency autocorrelation function for $s(t)$ is now developed. It expresses the time and frequency resolution characteristics jointly.

A signal, $s(t)$, which has its spectrum translated up in frequency by ν (Hz) can be written $s(t)e^{j2\pi\nu t}$. A two dimensional autocorrelation function can be obtained by inserting the factor $e^{j2\pi\nu t}$ into the integral in (2.1). There are several ways to define the autocorrelation function. The most common definition will be used here:

$$\phi(\tau, \nu) = \int_{-\infty}^{\infty} s(t - \frac{\tau}{2}) s^*(t + \frac{\tau}{2}) e^{-j2\pi\nu t} dt \quad (2.7)$$

For pulse trains of interest in this report, the time spacing between pulses is greater than the pulse duration. In addition, the time shift will always be small enough so that adjacent pulses of $s(t)$ will not correlate. Then, from (2.3), (2.4), and (2.7),

$$\phi(\tau, \nu) = \phi_o(\tau, \nu) \frac{\sin N\pi(\tau\Delta_f + \Delta_t\nu)}{N\sin\pi(\tau\Delta_f + \Delta_t\nu)}, \quad |\tau| < \Delta_t - T, \quad (2.8)$$

where $\phi_o(\tau, \nu)$ is the autocorrelation function for the waveform $w(t)$. Inserting $w(t)$ for $s(t)$ in (7) gives

$$\phi_o(\tau, \nu) = \begin{cases} \frac{\sin [\pi(BT + \nu T)(1 - \frac{|\tau|}{T})]}{\pi(BT + \nu T)}, & |\tau| \leq T \\ 0, & |\tau| > T \end{cases} \quad (2.9)$$

The autocorrelation function (2.8), in conjunction with (2.9), forms the basis for this report. All the waveform parameters appear in (2.8) and (2.9). Section 3.0 will discuss the selection of these parameters for designing waveforms with desired resolution properties.

$\phi(\tau, \nu)$ has been called the time-frequency autocorrelation function. In radar work it is normally called the ambiguity function. In that usage, range and velocity are the variables that usually appear as arguments. Target range and velocity manifest themselves as time delay and frequency shift respectively. It is shown in Appendix 6.1 that the time-range and frequency-velocity transformations are

$$\tau = \frac{2r}{c} \quad (2.10a)$$

$$\nu = \frac{2v}{c} f_c \quad (2.10b)$$

where r is the target range, v is target velocity, f_c is the radar carrier frequency and c is the speed of light.

3.0 WAVEFORM DESIGN

This section begins with an analysis of the structure of $\phi(\tau, \nu)$. Sidelobe weighting techniques are then discussed and design formulae for uniform coherent pulse trains are established.

3.1 Ambiguity Function Structure

The expression of interest is the magnitude of the auto-correlation function $\phi(\tau, \nu)$. Combining (2.8) and (2.9), this can be written in terms of the product of two factors.

$$|\phi(\tau, \nu)| = \left| \frac{\sin \left[\pi(B\tau + \nu T) \left(1 - \frac{|\tau|}{T}\right) \right]}{\pi(B\tau + \nu T)} \right| \left| \frac{\sin N\pi(\tau\Delta_f + \Delta_t\nu)}{N \sin \pi(\tau\Delta_f + \Delta_t\nu)} \right|, |\tau| \leq \Delta_t - T \quad (3.1)$$

The structure of the left factor, hereafter called the pulse factor, is examined first. This factor is dependent on only the basic pulse parameters B and T . In general, for practical radar waveforms, the values of B, T and ν are such that the denominator $(B\tau + \nu T)$ becomes very large before the factor $(1 - \frac{|\tau|}{T})$ differs significantly from unity. Therefore, a good approximation to the pulse factor in (3.1) is

$$\phi_o(\tau, \nu) = \frac{\sin \left[\pi(B\tau + \nu T) \left(1 - \frac{|\tau|}{T}\right) \right]}{\pi(B\tau + \nu T)} \approx \frac{\sin \pi(B\tau + \nu T)}{\pi(B\tau + \nu T)} \quad (3.2)$$

This function is zero whenever $B\tau + \nu T = \pm n$, where $n = 1, 2, \dots$. It has its peak value of unity where $B\tau + \nu T = 0$. These features are illustrated in Figure 3.1 which shows, as dashed lines, the loci of the zeros of ϕ_o in the (τ, ν) plane. Between each pair of dashed lines is a ridge or lobe. The main lobe passes through the center of the coordinates and has a width $2/B$ in the τ direction.

The structure of the right factor is similarly examined. This factor, hereafter called the array factor, is zero where $(\tau\Delta_f + \Delta_t\nu) = \frac{k}{N}$ for all integer values of k except those for which k/N is an integer. The magnitude of the array factor is unity when $(\tau\Delta_f + \Delta_t\nu) = \pm n, n = 0, 1, 2, \dots$. It is periodic in τ with period $\tau_p = 1/\Delta_f$ and periodic in ν with period $\nu_p = 1/\Delta_t$. It also has zeros with τ -periodicity $1/N\Delta_f$ and ν -periodicity $1/N\Delta_t$. The loci of the unity values for the array factor are shown as the straight lines in Figure 3.1. The loci of the zeros are not shown, but

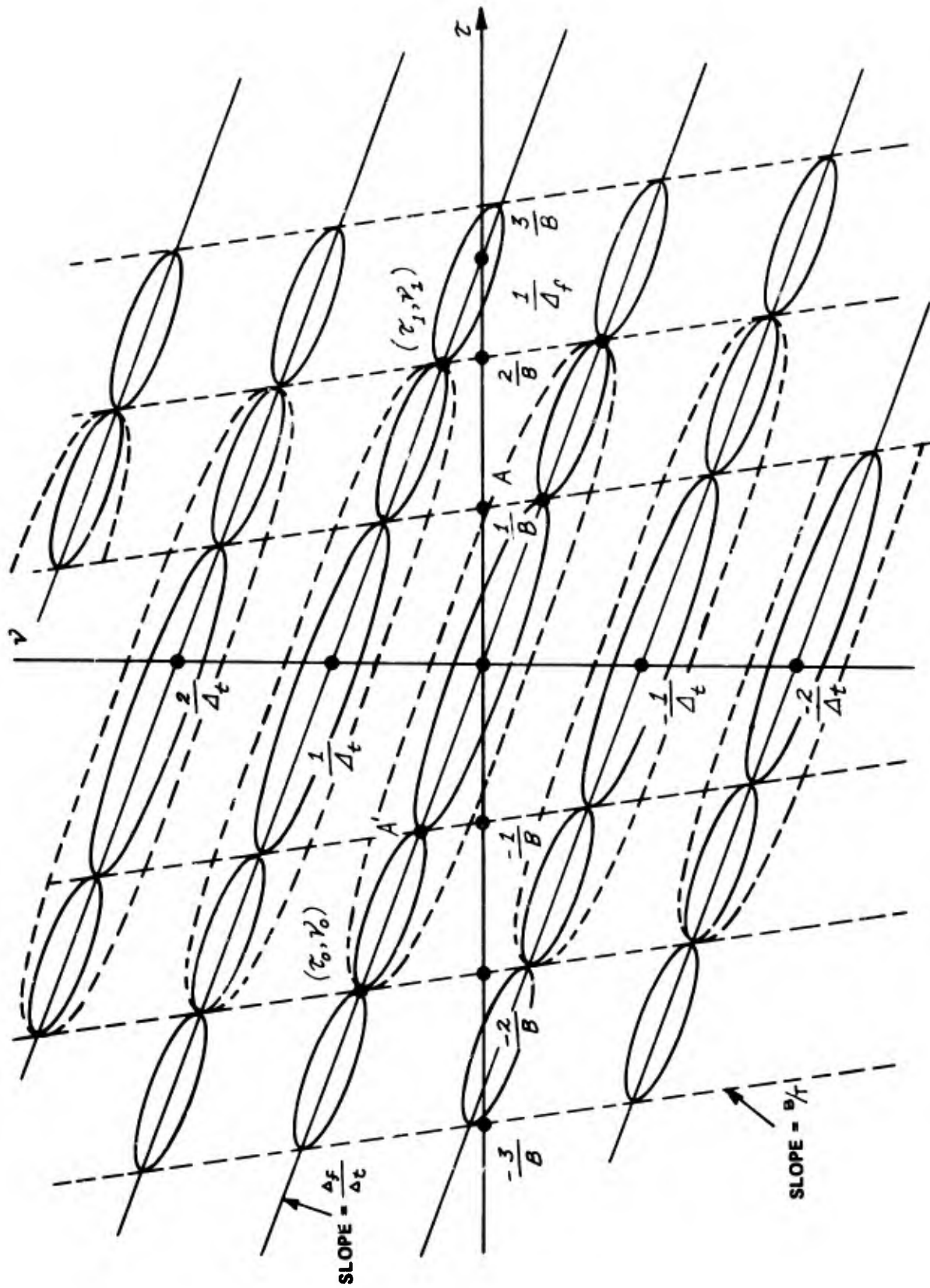


Figure 3.1 FREQUENCY JUMP BURST WAVEFORM AMBIGUITY FUNCTION

would appear as $N-1$ lines uniformly spaced between each pair of straight solid lines. The signal behavior illustrated in Figures 2.1 and 2.2 is manifest in (3.1) as the array factor.

The structure of the array factor along the τ -axis ($\nu=0$) is shown in Figure 3.2. Similarly shown is the structure of the pulse factor in (3.1).

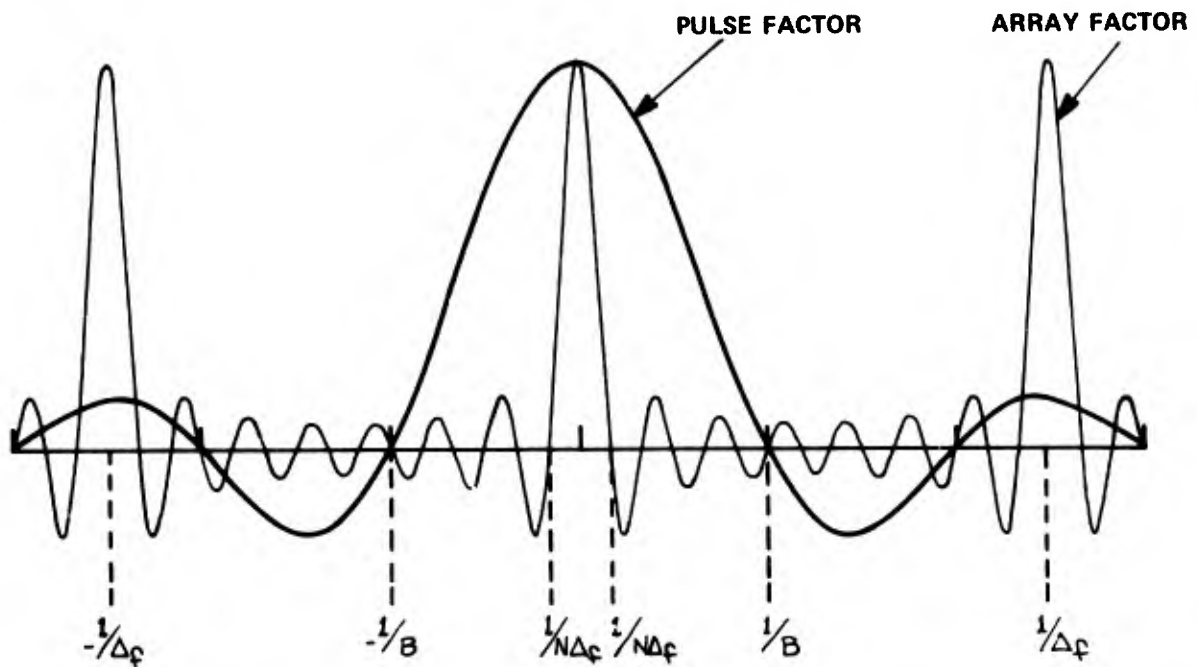


Figure 3.2 FACTORS OF THE AMBIGUITY FUNCTION

The parameters $\theta, \tau, \Delta_f, \Delta_t$ and N will generally be such that the array factor will have a much finer lobe structure than the pulse factor. When this situation prevails, it is convenient to view the array factor as a sampling function that is modulated by the pulse factor in order to give $\phi(\tau, \nu)$. With this interpretation of the behavior of the two factors in equation (3.1), the resultant $|\phi(\tau, \nu)|$ can be sketched in Figure 3.1.

Figure 3.1 shows, as the solid ellipses, the principal lobes of $\phi(\tau, \nu)$. These lobes represent the sampling of the pulse factor with

the main lobes of the array factor. The resultant structure is seen to be dominated by the array factor. That is, the time-frequency coupling is determined largely by parameters affecting only the array factor.

Figure 3.2 shows that $|\phi(\tau, \nu)|$ possesses many sidelobes in the vicinity of the main lobe. For a waveform to be most effective in typical radar environments, it should ideally be unimodal. Within practical constraints it is not possible to obtain a unimodal $\phi(\tau, \nu)$. It is possible, however, to reduce sidelobe strength relative to the main lobe strength so that sidelobe problems are greatly minimized if not eliminated. The next section discusses a technique for reducing sidelobes.

3.2 Single-Pulse Sidelobe Suppression

The most common of the techniques for reducing sidelobes makes use of what is called a transversal filter or transversal equalizer. The transversal filter, $h(t)$, can be characterized by its impulse response:

$$h(t) = \sum_{k=-M}^M a_k \delta(t - b_k) \quad (3.3)$$

where $\delta(t)$ is the unit impulse. For Hamming weighting, $M=1$, $a_1 = a_{-1} = 0.426$, $a_0 = 1$, $b_0 = 0$, and $b_1 = -b_{-1}$. Taylor weighting uses $M > 1$, $a_k = a_{-k}$ and $b_k = -b_{-k}$. Taylor weighting and Hamming weighting produce very similar results; therefore, only Hamming weighting will be considered.

The transversal filter exploits the periodicity inherent in the waveform sidelobe structure. This can be illustrated by example for a signal consisting of a single linear FM pulse. Let the autocorrelation for the signal be

$$\phi_0(\tau, \nu) = \frac{\sin \pi(B\tau + \nu T)}{\pi(B\tau + \nu T)} \quad (3.4)$$

(3.4) is obtained from (3.2). A profile of this function for constant ν is shown as a solid curve in Figure 3.3. When (3.4) is Hamming-filtered with $b_1 = \frac{1}{B}$, the weighted or equalized function, $\phi_{ow}(\tau, \nu)$, is

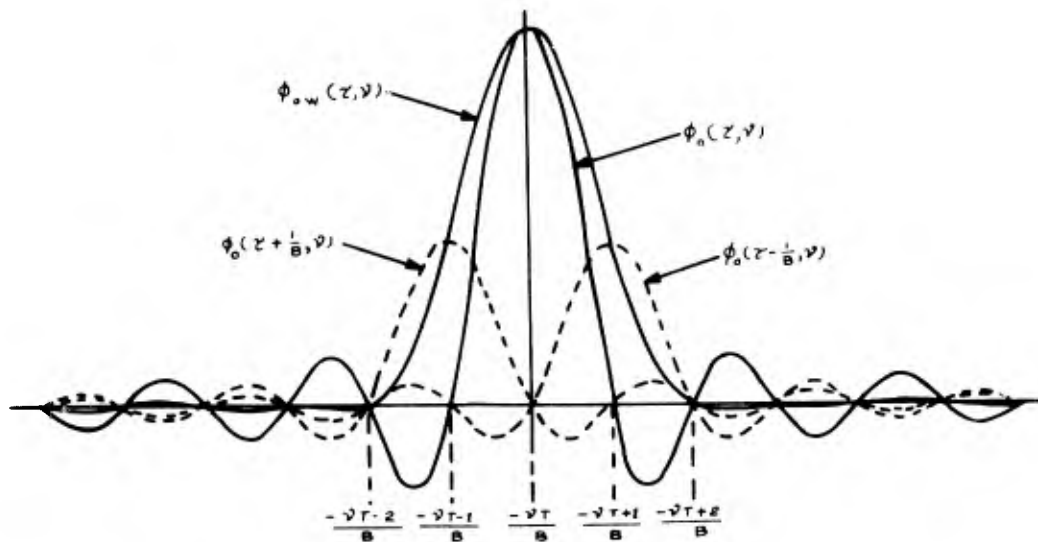


Figure 3.3 HAMMING WEIGHTING

$$\phi_{ow}(\tau, \nu) = 0.426 \phi_o\left(\tau + \frac{1}{B}, \nu\right) + \phi_o(\tau, \nu) + 0.426 \phi_o\left(\tau - \frac{1}{B}, \nu\right) \quad (3.5)$$

The amplitude-scaled and τ -translated waveforms are shown as the dashed curves in Figure 3.3. It is apparent that the technique of equalization is to use adjacent sidelobes for cancellation. It is also apparent that the width of the central lobe of $\phi_{ow}(\tau, \nu)$, also shown in Figure 3.3, is approximately twice that for $\phi(\tau, \nu)$. This is the penalty for reducing sidelobes.

The weighting constant $a_1 = 0.426$ is chosen for weighting a $\frac{\sin \chi}{\chi}$ structure. The result is that all sidelobes of $\phi(\tau, \nu)$ beyond the first are suppressed by at least 40 dB. Taylor weighting can be used to achieve a more uniform sidelobe level than Hamming weighting with a slightly narrower central lobe. The differences are small however. It should be noted that when a waveform does not have a $\frac{\sin \chi}{\chi}$ structure, but does have periodic sidelobes, the weighting constant a_1 should be adjusted from its nominal Hamming value to give the most desirable results. The autocorrelation function for the linear FM pulse given by equation (2.9) differs from the $\frac{\sin \chi}{\chi}$ form but, as was pointed out, for

typical values of pulse and target parameters, the approximation (3.2) is very good and Hamming weighting can be applied without alteration.

3.3 Sidelobe Suppression for Coherent Pulse Trains

The coherent pulse train has an autocorrelation structure that is more complex than that of a single pulse. Therefore, it is not possible to remove the unwanted sidelobes of the coherent pulse train as simply as for the single pulse. The same fundamental techniques are used in both cases however, and in this section a technique for weighting coherent pulse trains will be illustrated.

Equation (2.8) shows that the autocorrelation function for the coherent pulse train is a product of two factors, the first being the autocorrelation for the single pulse and the second, an autocorrelation function for a coherent sequence of uniformly spaced sinusoids. It is the second factor, the array factor, that reflects the properties of the "train." In many situations of interest and, in particular, for cases of interest here, parameters will be such that the array factor in (2.8) will vary much more rapidly than the pulse factor. Looking at Figure 3.2, this means that the product, $\phi(\tau, \nu)$, will possess approximately the same structure as the array factor in the vicinity of the central lobe of the array factor. This is the region of greatest interest. The sidelobe weighting required for this region of $\phi(\tau, \nu)$ is therefore the same as that required for weighting the array factor alone. Figure 3.2 also shows that the sidelobes of the pulse factor will appear in $\phi(\tau, \nu)$ because of the sampling of the pulse factor sidelobes by the array factor. These sidelobes can easily be reduced by weighting the pulse factor separately. This has negligible effect in the region of the central lobe of $\phi(\tau, \nu)$ because, under present assumptions, this region is dominated by the characteristics of the array factor.

The assumption that the array factor varies much more rapidly than the pulse factor is essential to the success of the weighting technique to be employed. It implies that the array factor and pulse factor can, in effect, be weighted separately and the resultant weighted

autocorrelation function for the pulse train will possess the same behavior in the region of the central lobe as the weighted autocorrelation function for a single pulse. Hence, "optimum" Hamming weighting can be achieved for the coherent pulse train.

To verify the applicability of Hamming weighting to the array factor, it should be shown that the array factor given in equation (2.8) closely approximates the $\frac{\sin \chi}{\chi}$ form in the vicinity of its main lobe. This can be seen easily when N is large, as will be assumed. In this case, the argument $(\tau \Delta_f + \Delta_t \nu)$ will be very small in the region of the main lobe, as determined by the numerator in (2.8). Then, the denominator can be approximated by $\sin \pi (\tau \Delta_f + \Delta_t \nu) \approx \pi (\tau \Delta_f + \Delta_t \nu)$

The pulse train is weighted by first weighting the individual pulses as in equation (3.5). When the pulses are weighted before the coherent summation, the resultant sum can be written as in equation (2.8).

$$\phi'(\tau, \nu) = \phi_{ow}(\tau, \nu) \frac{\sin N\pi(\tau \Delta_f + \Delta_t \nu)}{N \sin \pi(\tau \Delta_f + \Delta_t \nu)}, \quad |\tau| < \Delta_t - \tau \quad (3.5)$$

The sidelobes of $\phi_{ow}(\tau, \nu)$ are suppressed at least 40 dB. $\phi_{ow}(\tau, \nu)$ can be represented in Figure 3.1 by removing all the dashed straight lines except those crossing the τ -axis at $\tau = \pm \frac{2}{B}$. These parallel lines represent the approximate loci of the zeros defining the central and only significant lobe of $\phi_{ow}(\tau, \nu)$.

The second stage of weighting removes the sidelobes of $\phi_{ow}(\tau, \nu)$ in the vicinity of the central lobe. As shown previously, the structure of $\phi'(\tau, \nu)$ near its central lobe will be approximately the same as the structure of the array factor. Thus, the weighting applied to $\phi'(\tau, \nu)$ will be the same weighting as would be applied to the array factor in equation (3.5).

$$\phi_w(\tau, \nu) = 0.426 \phi'(\tau - \frac{1}{N\Delta_f}, \nu) + \phi'(\tau, \nu) + 0.426 \phi'(\tau + \frac{1}{N\Delta_f}, \nu) \quad (3.6)$$

$\phi_w(\tau, \nu)$ is the final result. It is characterized with a central lobe and adjacent sidelobes suppressed approximately 40 dB.

3.4 Near-Range Ambiguity Characteristics

In order to design a pulse train with desirable properties, it is necessary to quantitatively relate the pulse train parameters to the dimensions of $\phi_w(\tau, \nu)$. The necessary relationships are developed here.

In Figure 3.1, the dashed ellipses represent the principal lobes of $\phi'(\tau, \nu)$ which is given by equation (3.5). The final stage of weighting requires τ -shifts of $\pm \frac{1}{N\Delta_f}$. These shifts extend the extremes of the lobes in the τ direction by approximately $\pm \frac{1}{N\Delta_f}$. For $N\Delta_f$ sufficiently large, the extension will be very small and within the approximation that the main lobe of the pulse factor is doubled in τ -extent when the individual pulses are weighted. The coordinates indicating the extents of the main lobe and first ambiguous lobe are approximated as the points of intersection of the appropriate straight lines shown in figure 1.3:

$$\nu_0 = \frac{2\Delta_f}{B\Delta_t - \Delta_f T} \quad (3.7a)$$

$$\tau_0 = \frac{-2\Delta_t}{B\Delta_t - \Delta_f T} \quad (3.7b)$$

$$\nu_1 = \frac{B - 2\Delta_f}{B\Delta_t - \Delta_f T} \quad (3.7c)$$

$$\tau_1 = \frac{2\Delta_t - T}{B\Delta_t - \Delta_f T} \quad (3.7d)$$

Notice that the number of pulses, N , has no effect on the extent of the principal lobes. N does however affect the width of the lobes. The null-to-null width of the central lobe of $\phi'(\tau, \nu)$ along the τ axis is $\frac{2}{N\Delta_f}$. This width is approximately doubled when weighting is applied to $\phi'(\tau, \nu)$ so the resultant null-to-null width for $\phi_w(\tau, \nu)$ is

$$W_\tau = \frac{4}{N\Delta_f} \quad (3.8a)$$

Similarly, the null-to-null width of $\phi_w(\tau, \nu)$ along the ν -axis is

$$W_\nu = \frac{4}{N\Delta_t} \quad (3.8b)$$

For design purposes, equations (3.7) and (3.8) completely specify the autocorrelation function in terms of the pulse train parameters. The use of these expressions for the calculation of autocorrelation properties of pulse trains for the TRADEX system appears in Appendix 6.4.

3.5 Far-Range Ambiguity Characteristics

In this section, additional properties of the coherent pulse train are considered.

The analyses and properties previously developed apply to the case where $\tau \leq \Delta_t - T$. For τ beyond this range, the results obtained no longer apply. The critical problem that arises when $\tau > \Delta_t - T$ is that strong ambiguous range sidelobes appear. This is because, for certain values of τ there will be cross correlation between pulses when the pulses overlap in frequency. This characteristic can be illustrated with the help of Figure 3.4, which is a schematic representation of the pulse train. The straight line segments represent the individual pulses.

Figure 3.4 shows two pulse trains, one marked by solid lines and the other marked by dashed lines. When one train is shifted an amount $\tau = \Delta_t - \Delta_f \frac{T}{B}$, it is apparent that there will be strong correlation between adjacent pulses. This correlation appears as an ambiguity lobe

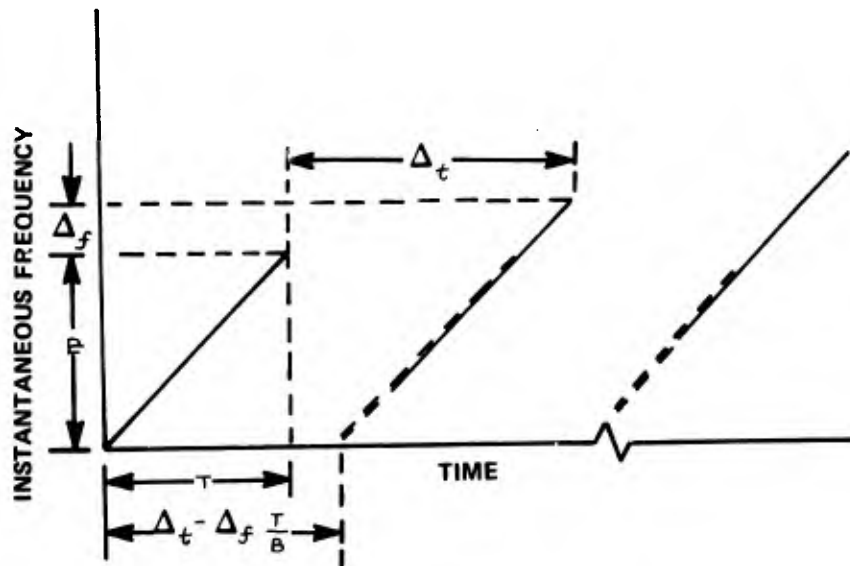


Figure 3.4 ORIGIN OF FAR-RANGE AMBIGUITIES

far beyond the τ range included in figure 3.1. Additional range ambiguities will appear at multiples of $\tau = \Delta_t - \Delta_f \frac{T}{B}$ until τ is sufficiently large that pulse spectra can no longer overlap. The ambiguous delay interval is then given very closely as

$$\tau_a = \Delta_t - \Delta_f \frac{T}{B} \quad (\Delta_f < B) \quad (3.9)$$

The existence of these extended range ambiguities limits the use of coherent pulse trains to environments where the target extent is less than τ_a .

A seemingly obvious cure is to increase the frequency spacing so that these extended range ambiguities can be removed entirely. To see that this is not an acceptable remedy refer to figure 3.1. Notice that the central lobe and its adjacent ambiguity lobe may overlap in ν or, equivalently, doppler; that is, $\nu_1 < \nu_0$. In fact $\nu_1 < 0$ is possible. This is not desirable because it means that targets can exhibit ambiguous responses. To prevent these ambiguity problems, it is necessary to have $\nu_1 > 0$ and certainly sufficient to have $\nu_1 \geq \nu_0$. From the first condition and equation (3.7c), $\Delta_f < \frac{B}{2}$; from the second condition and equations (3.7a) and (3.7c), $\Delta_f \leq \frac{B}{4}$. Thus, the frequency spacing between pulses will necessarily be less than the pulse bandwidth and extended range ambiguities will exist. Equation (3.9) provides another design relation that is useful when the locations of the extended ambiguities can be a problem.

4.0 SYSTEMS CONSIDERATIONS

This chapter examines a few systems problems that arise in the implementation of coherent pulse trains. In particular, the effects of the quantization of pulse data samples and non-uniform pulse sampling are investigated.

4.1 Quantization Errors

In certain radar systems the video or matched filter output is sampled and subsequent signal processing is performed with these data samples. When the signal processing is done digitally, as is often the case, the question of quantization errors arises naturally. The manner in which the quantization occurs is unimportant with respect to its consequences. It will be assumed that all the quantization occurs in the digitization of the video samples. The effects of these quantization errors on the structure of $\phi_w(\tau, \nu)$ are then calculated. It will not be necessary to work directly with $\phi_w(\tau, \nu)$. Instead, the effects of quantization on the structure of $\phi_{ow}(\tau, \nu)$ are evaluated. The extension of these results to $\phi_w(\tau, \nu)$ is straightforward.

The complex low-pass video is $\phi_{ow}(\tau, \nu)$. This can be represented in terms of its amplitude and phase,

$$\phi_{ow}(\tau, \nu) = a(\tau, \nu) e^{j\theta(\tau, \nu)} \quad (4.1)$$

The video includes the amplitude and phase factors, so that two samplers are operating simultaneously. The sampling interval is T_s and is assumed to be the Nyquist interval. The sampled signal is

$$\phi_{ow}(nT_s, \nu) = a(nT_s, \nu) e^{j\theta(nT_s, \nu)} \quad (4.2)$$

When $\phi_{ow}(nT_s, \nu)$ is quantized, the resulting quantized samples can be written

$$\hat{\phi}_{ow}(nT_s, \nu) = [a(nT_s, \nu) + \epsilon_a(nT_s)] e^{j[\theta(nT_s, \nu) + \epsilon_\theta(nT_s)]} \quad (4.3)$$

where $\epsilon_a(nT_s)$ and $\epsilon_\theta(nT_s)$ are the amplitude and phase quantization errors respectively. In order to study the effects of the quantization errors it will be assumed that $\hat{\phi}_{ow}(nT_s, \nu)$ undergoes a reconstruction process to recreate $\phi_{ow}(\tau, \nu)$. The reconstruction process applied to $\hat{\phi}_{ow}(nT_s, \nu)$ is the same process which, when applied to $\phi_{ow}(nT_s, \nu)$, will reproduce $\phi_{ow}(\tau, \nu)$ without error. The error between $\phi_{ow}(\tau, \nu)$ and the reconstruction from $\hat{\phi}_{ow}(nT_s, \nu)$ is used to qualify the effects of quantization.

The assumption regarding the quantization errors are that:

- 1) amplitude and phase quantization errors are independent,
- 2) amplitude and phase quantization errors are zero mean and independent from sample to sample
- 3) $\overline{\epsilon_a^2(nT_s)} = \sigma_a^2$
 $\overline{\epsilon_\theta^2(nT_s)} = \sigma_\theta^2$
where $\overline{(\cdot)}$ denotes expectation,
- 4) phase quantization errors are small (less than, say, 0.1 rad.).

With these assumptions, it is shown in Appendix 6.2 that the mean squared error between $\phi_{ow}(\tau, \nu)$ and $\hat{\phi}_{ow}(\tau, \nu)$, the reconstruction based upon $\hat{\phi}_{ow}(nT_s, \nu)$, is

$$\begin{aligned} \overline{|e(\tau, \nu)|^2} &= \sigma_a^2(1 + \sigma_\theta^2) \sum_{n=-\infty}^{\infty} U(nT_s) \left[\frac{\sin \pi(\frac{\tau}{T_s} - n)}{\pi(\frac{\tau}{T_s} - n)} \right]^2 \\ &\quad + \sigma_\theta^2 \sum_{n=-\infty}^{\infty} a^2(nT_s, \nu) \left[\frac{\sin \pi(\frac{\tau}{T_s} - n)}{\pi(\frac{\tau}{T_s} - n)} \right]^2 \end{aligned} \quad (4.4)$$

where $U(nT_s) = 1$ wherever $a(nT_s)$ is non-zero, and zero elsewhere. It is also true that

$$\overline{|\phi_{ow}(\tau, \nu)|^2} = \overline{|\phi_{ow}(\tau, \nu)|^2} + \overline{|e(\tau, \nu)|^2} \quad (4.5)$$

indicating that the error is in quadrature with $\phi_{ow}(\tau, \nu)$.

Equation (4.4) shows that the quantization error depends upon the signal structure. In particular, the phase quantization results

in an error component whose structure is directly related to $a(\tau, \nu)$.

In order to gain some quantitative measure of quantization effects it has been assumed that $\phi_{ow}(\tau, \nu)$ has a raised cosine shape in τ . In particular,

$$\phi_{ow}(\tau, \nu) = a(\tau) = \begin{cases} \cos^2 \frac{\pi \tau}{2}, & |\tau| \leq 1 \\ 0 & \text{elsewhere} \end{cases} \quad (4.6a)$$

and

$$u(\tau) = \begin{cases} 1, & |\tau| \leq 1 \\ 0 & \text{elsewhere} \end{cases} \quad (4.6b)$$

The error terms in equation (4.4) were evaluated separately and plotted in Appendix 6.2 as the normalized mean square error due to amplitude quantization ($e_a^2(\tau) = \frac{1}{\sigma_a^2} |e(\tau, 0)|^2 |_{\sigma_\theta=0}$) and normalized mean square error due to phase quantization ($e_\theta^2(\tau) = \frac{1}{\sigma_\theta^2} |e(\tau, 0)|^2 |_{\sigma_a=0}$). The value of T_s is 1/2 which is considered adequate for reconstructing $a(\tau)$.

$$e_a^2(\tau) = \sum_{n=-\infty}^{\infty} u(nT_s) \left[\frac{\sin \pi \left(\frac{\tau}{T_s} - n \right)}{\pi \left(\frac{\tau}{T_s} - n \right)} \right]^2 \quad (4.7a)$$

$$e_\theta^2(\tau) = \sum_{n=-\infty}^{\infty} a(nT_s) \left[\frac{\sin \pi \left(\frac{\tau}{T_s} - n \right)}{\pi \left(\frac{\tau}{T_s} - n \right)} \right]^2 \quad (4.7b)$$

As long as (4.6) represents a good approximation to the actual $a(\tau)$, the curves of $e_a^2(\tau)$ and $e_\theta^2(\tau)$ may be applied universally to evaluate average errors for any system when σ_a^2 and σ_θ^2 are known. When the quantization intervals have widths Δa and $\Delta \theta$ for amplitude and phase respectively and the quantization errors are assumed to be uniformly distributed within the intervals:

$$\sigma_a^2 = \frac{(\Delta a)^2}{12} \quad (4.8a)$$

$$\sigma_\theta^2 = \frac{(\Delta \theta)^2}{12} \quad (4.8b)$$

$\Delta \theta$ is understood to be in radians and Δa is the normalized quantization interval (normalized to the peak of $a(\tau)$).

It has been found that for $\Delta\theta \approx 0.1$ radian and $\Delta a = 0.1$ (a rather coarse quantization), the effects of quantization on $\phi_{ow}(\tau, \nu)$ are no worse than a few dB increase in range-time sidelobes that are on the order of -40dB.

The effect of quantization errors upon the autocorrelation function $\phi_w(\tau, \nu)$ is easily calculated. If the quantization errors are assumed independent from pulse to pulse, when the pulses are coherently summed the respective errors will be summed as though they are incoherent. The resultant pulse amplitude is N times that of the single pulse and the resultant pulse power is N^2 times that of the single pulse. Because the errors add incoherently their resultant average power is N times that of a single error. Thus, there is a relative error power decrease of $1/N$ when going from a single pulse to the coherent train. The structure of the resultant error pattern is the same as that indicated by equation (4.4) so calculations are readily performed.

4.2 Sampling Errors

A system problem that is peculiar to certain data processing systems concerns the sampling procedures. This problem is not peculiar to the implementation of coherent pulse trains; rather, it is a fundamental problem in sampling.

The video output, $\phi_o(\tau, \nu)$, is sampled before further processing is performed. When the bandwidth of $\phi_o(\tau, \nu)$ is large, it is difficult to build samplers that can operate as fast as the required Nyquist rate. A means for avoiding this construction problem is to build lower rate samplers and interleave them so that, in effect, the required sampling rate is achieved. This solution creates an additional problem, namely; What does one do when the samplers are incorrectly synchronized so the samples are not uniformly spaced? Fortunately this problem has a simple solution. When the relative offset between the samplers is known, there is no information lost in the sampling sequence and a uniformly spaced sample sequence can be generated from the original sample sequence. The particular case of interest is that in which two samplers are used, each operating at one half the Nyquist rate.

The sampling interval for each sampler is T_0 . The output of the first sampler is (the ν^- dependence is suppressed here for brevity)

$$\phi_{01}(\tau) = \sum_{n=-\infty}^{\infty} \phi_0(nT_0) \delta(\tau - nT_0) \quad (4.9a)$$

The second sampler is delayed Δ seconds with respect to the first and provides the output

$$\phi_{02}(\tau) = \sum_{n=-\infty}^{\infty} \phi_0(nT_0 + \Delta) \delta(\tau - \Delta - nT_0) \quad (4.9b)$$

The Nyquist interval is $T_s = T_0/2$. In Appendix 6.3 it is shown that $\phi_0(\tau)$ can be reconstructed without error from the sequences $\phi_{01}(\tau)$ and $\phi_{02}(\tau)$ and that the reconstruction process is given by

$$\begin{aligned} \phi_0(\tau) = \sum_{n=-\infty}^{\infty} & \left\{ \phi_0(nT_0) \frac{\sin \pi \left(\frac{\tau}{T_s} - 2n \right)}{\pi \left(\frac{\tau}{T_s} - 2n \right)} + \phi_0(nT_0 + \Delta) \frac{\sin \pi \left(\frac{\tau - \Delta}{T_s} - 2n \right)}{\pi \left(\frac{\tau - \Delta}{T_s} - 2n \right)} \right. \\ & \left. - \frac{2}{\tan \left(\frac{\pi \Delta}{2T_s} \right)} \left[\phi_0(nT_0) \frac{\sin \frac{2\pi}{2} \left(\frac{\tau}{T_s} - 2n \right)}{\frac{\pi}{2} \left(\frac{\tau}{T_s} - 2n \right)} - \phi_0(nT_0 + \Delta) \frac{\sin^2 - \frac{\pi}{2} \left(\frac{\tau - \Delta}{T_s} - 2n \right)}{\frac{\pi}{2} \left(\frac{\tau - \Delta}{T_s} - 2n \right)} \right] \right\} \quad (4.10) \end{aligned}$$

The conclusion is that no matter what the offset Δ , $\phi_0(\tau)$ can, in principle, be recovered without error. The term in square brackets in (4.10) can be regarded as the error correction due to non-uniform sampling. Indeed, when $\Delta = T_0/2 = T_s$ this term is zero. Since $\phi_0(\tau)$ can be recovered without error it is possible, when digitally processing, to use (4.10) to regenerate a uniformly spaced sample sequence by evaluating (4.10) at $\tau = mT_s$, $m = 0, \pm 1, \pm 2, \dots$

5.0 SUMMARY

A detailed analysis of the properties of uniform coherent pulse trains was presented. The restriction to uniform interpulse shifts in time and frequency permitted simple formulae to be derived for the dimensions of the ambiguity function in terms of fundamental parameters.

The pulse train was shown to have resolution properties equivalent to a single pulse with the same overall time duration and bandwidth. Unlike a single FM pulse, the pulse train exhibited extended range ambiguities. The suppression of these ambiguities was not discussed, except to show why a seemingly obvious suppression technique would not be satisfactory. A possible approach to the suppression of these ambiguities is to phase code the pulses in the train. This can be a subject for further study.

The analyses also showed that the gross structure of the waveform ambiguity function is determined by the array factor which is a function of the pulse repetition interval, the frequency step, and the number of pulses. The time-frequency coupling for the waveform is the time-frequency coupling for the array factor, $\tau = \frac{\Delta t}{\Delta f} \nu$. The alteration of the time frequency coupling was not discussed. This is an important problem because if the velocity of the target can not be adequately determined, then neither can the range; consequently, the range error will be determined by the degree of time-frequency coupling. This problem is minimized if the waveform is insensitive to doppler or frequency shift. Increased insensitivity could be obtained by altering the time-frequency shift pattern of pulses in the train; this alters the array factor. A detailed study of this technique is another subject for future study.

The systems problems considered were rather specific and well-defined. The sensitivity of the reconstruction technique for non-uniformly spaced samples was not considered. It is expected that the technique is sensitive to quantization errors when the offset, Δ , is very large ($\Delta \approx T_0$) or small ($\Delta \approx 0$). This should be an unlikely situation. If it proves to be otherwise, an analysis of the quantization effects can be readily performed.

6.0 APPENDICES

6.1 Properties of the Return Signal

The time delay-range and doppler shift-velocity relationships are formalized on a physical basis. The meaning of equation 2.7 is thereby established.

Consider a radar target which, at time $t = 0$, is at a range R from the radar and moving with constant velocity v toward the radar. If an impulse is transmitted at time t , it can be easily shown that it will be returned to the radar τ_d seconds later where

$$\tau_d = \frac{2R/c}{1+v/c} - \frac{2v/c}{1+v/c} t \quad (6.1)$$

Define

$$\tau = \frac{2R/c}{c} \quad (6.2a)$$

and

$$\beta = \frac{v/c}{c} \quad (6.2b)$$

so that

$$\tau_d = \frac{\tau}{1+\beta} - \frac{2\beta t}{1+\beta}$$

The point target can be characterized by its impulse response which is simply a delay. The response at time t to an impulse transmitted at time t' is denoted $h(t, t')$. Then $h(t, t') = \delta(t - t' - \tau_d)$ and the returned waveform can be written

$$r(t) = \int_{-\infty}^{\infty} s(t') h(t, t') dt' = \int_{-\infty}^{\infty} s(t') \delta(t - t' - \tau_d) dt' \quad (6.3)$$

Substituting (6.1) into (6.3) and integrating,

$$r(t) = \left(\frac{1+\beta}{1-\beta} \right) s \left[\left(\frac{1+\beta}{1-\beta} \right) t - \frac{\tau}{1-\beta} \right] \quad (6.4)$$

(6.4) shows that the return is an amplitude-scaled, time compressed and delayed replica of the transmitted signal. The amplitude factor can be

disregarded because it has no effect on the structure of the autocorrelation function (its presence is proper, however, and it has been shown to be relativistically correct). The effect of time compression must be examined.

If $s(t)$ has a time duration T then the time duration of $r(t)$ is T_r where $\left(\frac{1+\beta}{1-\beta}\right)T_r = T$. The time compression of $s(t)$ is $T - T_r = \frac{2\beta T}{1+\beta}$. This compression can be significant. To see when it can be disregarded recall that the return $r(t)$ will be correlated with a replica of $s(t)$. Now, if $s(t)$ has absolute bandwidth W , it cannot change significantly in a time period $\frac{1}{W}$. Therefore, to preserve the structure of the correlation function it is necessary for the time compression to be less than $\frac{1}{W}$.

$$2\beta T \approx \frac{2\beta T}{1+\beta} < \frac{1}{W} \quad (6.5)$$

or

$$2\beta TW < 1$$

When (6.5) is satisfied, as it almost always is, $r(t)$ is approximated very closely as a time delayed and frequency translated replica of $s(t)$. Condition (6.5) is called the quasi-stationary condition and is tacitly assumed in most radar analyses. It is equivalent to making the inconsistent assumptions that the target maintains a fixed range and a fixed velocity during the period of interaction with the radar pulse. This inconsistency simplifies analyses and is usually perfectly acceptable. As can be seen from 6.5, the validity of the quasi-stationary assumption becomes more questionable as the TW product of the waveform increases. This point is labored here because current technology permits the generation of TW products which violate the quasi-stationary assumption. In particular, the coherent pulse trains studied in this report have very high TW products. A typical coherent pulse train of interest will have $T = 50 \mu\text{sec}$, $W = 240 \text{ Mhz}$. If the target velocity $v = 7 \text{ km/sec}$, then $2\beta TW = 0.42$, indicating that the quasi-stationary assumption is barely met.

The transformations (2.10a) and (2.10b) can now be readily established. In (6.4), the amplitude factor can be assumed to be unity.

Since $\beta \ll 1$, the approximations $\frac{1+\beta}{1-\beta} \approx 1+2\beta$ and $\frac{1}{1-\beta} \approx 1+\beta$ are very good. Applying these approximations to (6.4) gives

$$r(t) \approx s \left[(t-\tau) + 2\beta t \right] \quad (6.6)$$

Since $s(t) = w(t) e^{j\omega_c t}$, the return becomes

$$r(t) = w \left[(t-\tau) + 2\beta t \right] e^{j\omega_c (t-\tau)} e^{j2\beta\omega_c t} \quad (6.7)$$

where $w(t)$ is a low pass signal (the complex envelope of $s(t)$) with a bandwidth much less than ω_c . In this case, as long as the time duration T_w of $w(t)$ is not very long, the low pass signal will suffer negligible distortion due to time compression ($2\beta T_w \omega_w \ll 1$ for $w(t)$) where T_w and ω_w are the time duration and bandwidth respectively for $w(t)$ and the additional approximation is valid:

$$r(t) \approx w(t-\tau) e^{j2\beta\omega_c t} e^{j\omega_c (t-\tau)} \quad (6.8)$$

Then, from (6.8) can be written

$$r(t) \approx s(t-\tau) e^{j2\pi\nu t} e^{j\gamma} \quad (6.9)$$

where $\nu = \frac{\beta\omega_c}{\pi} = \frac{2v}{\lambda}$ and γ is constant. Subject to proper assumptions it is apparent that the radar return can be regarded as a time delayed and frequency shifted replica of the transmitted waveform. The correlation between $s(t)$ and $r(t)$ is clearly represented by equation (2.7). Notice that the absolute phase of the return is not preserved, but since this phase is subject to many uncertainties, including the target scattering characteristics and propagation effects, it is not useful to preserve this quantity.

6.2 Analysis of Quantization Errors

The error expressions for quantization errors are derived.

When the phase quantization error is small, the exponential term in (4.3) can be approximated as $e^{j\epsilon_\theta(nT)} \approx 1 + j\epsilon_\theta(nT)$. Then (4.3)

can be rewritten as

$$\begin{aligned}\hat{\phi}_{ow}(nT_s, \nu) &= a(nT_s, \nu) e^{j\theta(nT_s)} + \left[\epsilon_a(nT_s) + j(a(nT_s)\epsilon_o(nT_s) + \epsilon_a(nT_s)\epsilon_\theta(nT_s)) \right] e^{j\theta(nT_s)} \\ &= \phi_{ow}(nT_s, \nu) + \left[\epsilon_a(nT_s) + j(a(nT_s)\epsilon_o(nT_s) + \epsilon_a(nT_s)\epsilon_\theta(nT_s)) \right] e^{j\theta(nT_s)}\end{aligned}\quad (6.10)$$

The error term is clearly evident in (6.10).

Any function $x(\tau)$ can be reconstructed from its samples $x(nT_s)$, when T_s is the Nyquist interval for $x(\tau)$ and $x(\tau)$ satisfies some other mathematical requirements that are of no concern here. The reconstruction process is specified below:

$$x(\tau) = \sum_{n=-\infty}^{\infty} x(nT_s) \frac{\sin \pi \left(\frac{\tau}{T_s} - n \right)}{\pi \left(\frac{\tau}{T_s} - n \right)} \quad (6.11)$$

Applying the reconstruction process to (6.10) gives

$$\hat{\phi}_{ow}(\tau, \nu) = \phi_{ow}(\tau, \nu) + \sum_{n=-\infty}^{\infty} \left[\epsilon_a(nT_s) + j(a(nT_s)\epsilon_o(nT_s) + \epsilon_a(nT_s)\epsilon_\theta(nT_s)) \right] e^{j\theta(nT_s)} \frac{\sin \pi \left(\frac{\tau}{T_s} - n \right)}{\pi \left(\frac{\tau}{T_s} - n \right)} \quad (6.12)$$

From (6.12), the mean squared error $\overline{|\hat{\phi}_{ow}(\tau, \nu) - \phi_{ow}(\tau, \nu)|^2}$ is found and is given by equation (4.4).

If the summation term in (6.12) is written as $e(\tau, \nu)$ (6.12) gives

$$\begin{aligned}\overline{|\hat{\phi}_{ow}(\tau, \nu)|^2} &= \overline{|\phi_{ow}(\tau, \nu)|^2} + \overline{e(\tau, \nu)\phi_{ow}^*(\tau, \nu)} \\ &\quad + \overline{e^*(\tau, \nu)\phi_{ow}(\tau, \nu)} + \overline{|e(\tau, \nu)|^2}\end{aligned}\quad (6.13)$$

From (6.12) and the assumptions regarding the quantization errors, it follows that $\overline{e(\tau, \nu)} = 0$ and equation (4.5) results.

In Figures 6.1 and 6.2, the normalized mean square error due to amplitude quantization and due to phase quantization are given for the raised-cosine signal described in Section 4.1, equations (4.6), for a sampling rate which is 1/4 the null-to-null width, a value considered adequate for reconstructing the signal. The quantities given in the figures are normalized to the variances of the quantization errors, which are themselves small quantities, i. e. typically

$$\sigma_a^2 = 0.0033 a^2(\theta) \text{ for } \pm 0.1 a(\theta) \text{ amplitude quantization } (\Delta_a = 0.2)$$

$$\sigma_\theta^2 = 0.0037 (\text{rad})^2 \text{ for } \pm 6^\circ \text{ phase quantization } (\Delta_\theta = 12^\circ)$$

so that, in each case, a value of unity on the figure corresponds to an error which is about 24.5 dB smaller than the peak of the signal.

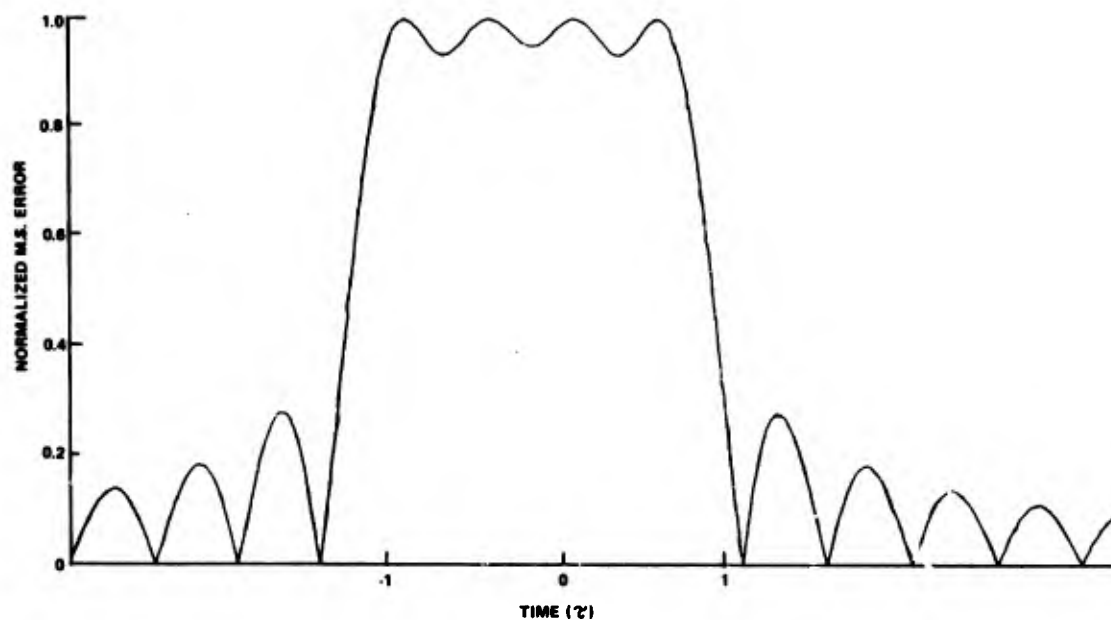
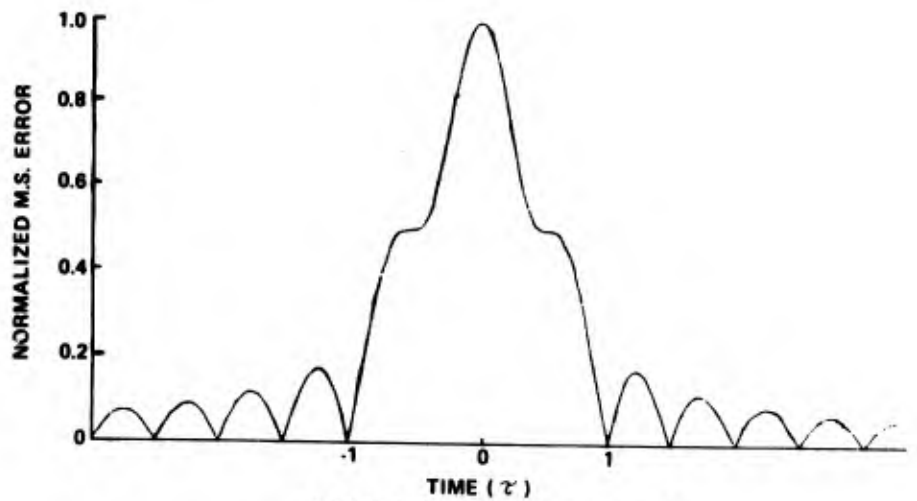
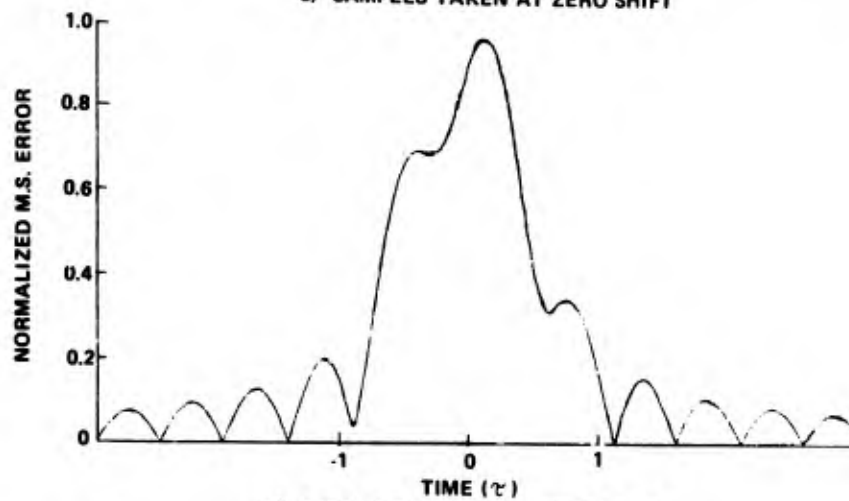


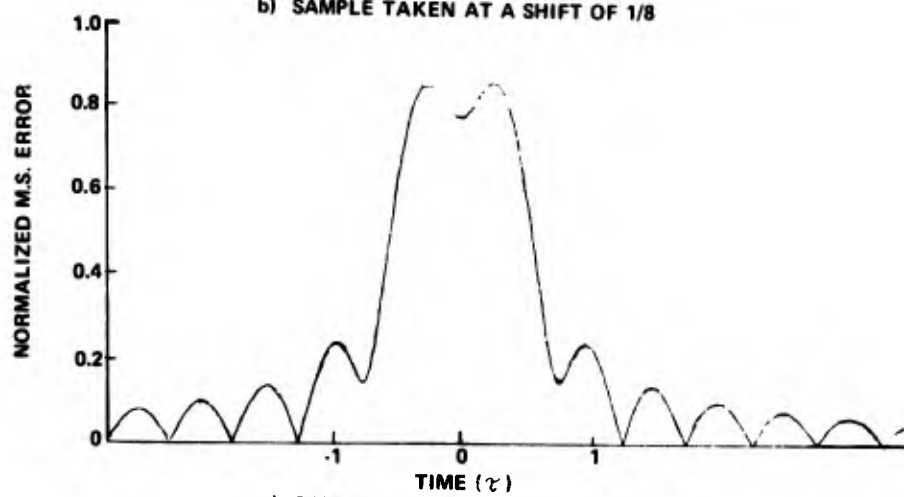
Figure 6.1 NORMALIZED MEAN SQUARE ERROR DUE TO AMPLITUDE QUANTIZATION (INDEPENDENT OF SAMPLE SHIFT)



a) SAMPLES TAKEN AT ZERO SHIFT



b) SAMPLE TAKEN AT A SHIFT OF 1/8



c) SAMPLES TAKEN AT A SHIFT OF 1/4

Figure 6.2 NORMALIZED MEAN SQUARE ERROR DUE TO PHASE QUANTIZATION. (EVALUATED AT SEVERAL TIME-SHIFTS OF SAMPLING POINT WITH RESPECT TO SIGNAL PEAK LOCATION)

6.3 Analysis of Sampling Errors

The reconstruction formula (4.10) is derived.

Let the Fourier transform of $\phi_o(\tau)$ be $\Phi_o(\omega)$. $\Phi_o(\omega)$ is assumed to be bandlimited to $\pm B/2$ rad/sec so that the Nyquist interval is $T_s = \frac{2\pi}{B}$ sec. It can be shown ⁽¹⁾ that the Fourier transforms of $\phi_{o1}(\tau)$ and $\phi_{o2}(\tau)$ are

$$\Phi_{o1}(\omega) = \frac{1}{T_o} \sum_{n=-\infty}^{\infty} \Phi_o\left(\omega + \frac{2\pi n}{T_o}\right) \quad (6.14a)$$

$$\Phi_{o2}(\omega) = \frac{1}{T_o} \sum_{n=-\infty}^{\infty} e^{j \frac{2\pi n \Delta}{T_o}} \Phi_o\left(\omega + \frac{2\pi n}{T_o}\right) \quad (6.14b)$$

$\Phi_{o1}(\omega)$ and $\Phi_{o2}(\omega)$ are the sums of shifted spectra. The magnitudes of the component spectra in $\Phi_{o1}(\omega)$ and $\Phi_{o2}(\omega)$ are illustrated in Figure 6.1.

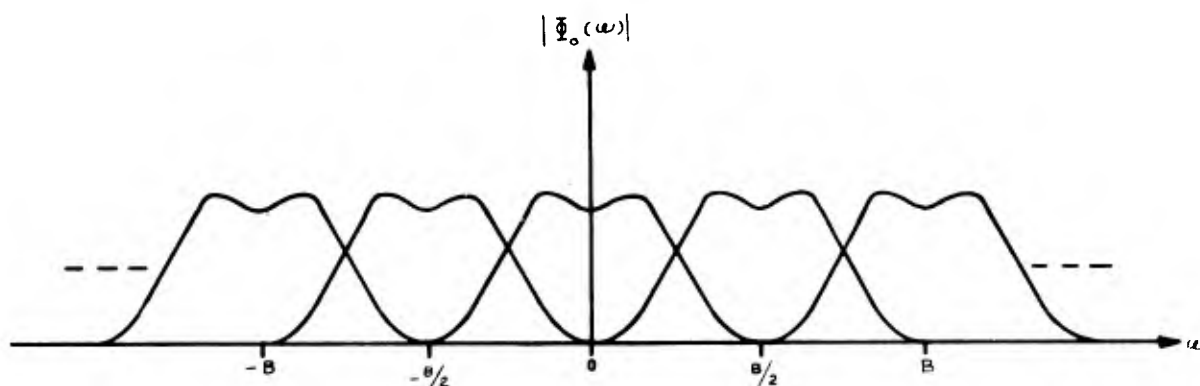


Figure 6.3 SPECTRUM OF SIGNAL SAMPLED AT 1/2 NYQUIST RATE

(1) A. Papoulis, "The Fourier Integral and Its Application," New York: McGraw-Hill, 1962.

The spectrum of $\phi_o(\tau)$ is wholly contained in the interval $[-\frac{B}{2}, \frac{B}{2}]$. However, the adjacent shifted spectra interfere with $\Phi(\omega)$ in this interval. Notice that the component spectra in $\Phi_{o2}(\omega)$ are distinguished from the corresponding component spectra in $\Phi_{o1}(\omega)$ by the presence of the exponential phase factors. This fact can be exploited to recover $\Phi_o(\omega)$ in the interval $[-\frac{B}{2}, \frac{B}{2}]$. Without laboring over detail, the technique is outlined.

Consider the restrictions of $\Phi_{o1}(\omega)$ and $\Phi_{o2}(\omega)$ to the interval $[0, \frac{B}{2}]$. These restrictions are

$$\Phi_{o1}(\omega) = \frac{1}{T_o} \Phi_o(\omega) + \frac{1}{T_o} \Phi_o(\omega - \frac{2\pi}{T_o}) ; 0 \leq \omega \leq \frac{B}{2} \quad (6.15a)$$

$$\Phi_{o2}(\omega) = \frac{1}{T_o} \Phi_o(\omega) + \frac{1}{T_o} e^{-j \frac{2\pi\Delta}{T_o}} \Phi_o(\omega - \frac{2\pi}{T_o}) ; 0 \leq \omega \leq \frac{B}{2} \quad (6.15b)$$

(6.15a) and (6.15b) can be solved simultaneously to give $\Phi_o(\omega)$ in terms of only $\Phi_{o1}(\omega)$ and $\Phi_{o2}(\omega)$. This solution is valid only for $0 \leq \omega \leq \frac{B}{2}$. The restriction of (6.14a) and (6.14b) to the interval $[-\frac{B}{2}, 0]$ are then used in the same way to obtain $\Phi_o(\omega)$ in that interval. When the components of $\Phi_o(\omega)$ thus obtained are combined, the entire spectrum is found, and can be written

$$\Phi_o(\omega) = \frac{T_o}{2} \left[\Phi_{o1}(\omega) + \Phi_{o2}(\omega) \right] H(\omega) - \frac{T_o}{2} \left[\Phi_{o1}(\omega) - \Phi_{o2}(\omega) \right] \frac{[H_1(\omega) - H_2(\omega)]}{j \tan \frac{\pi\Delta}{2T_s}} \quad (6.16)$$

where

$$H_1(\omega) = \begin{cases} 1 & ; \quad |\omega - \frac{B}{4}| \leq \frac{B}{4} \\ 0 & \text{elsewhere} \end{cases} \quad (6.17a)$$

$$H_2(\omega) = \begin{cases} 1 & ; \quad |\omega + \frac{B}{4}| \leq \frac{B}{4} \\ 0 & \text{elsewhere} \end{cases} \quad (6.17b)$$

$$H(\omega) = H_1(\omega) + H_2(\omega) = \begin{cases} 1 & ; \quad |\omega| \leq \frac{B}{2} \\ 0 & \text{elsewhere} \end{cases} \quad (6.17c)$$

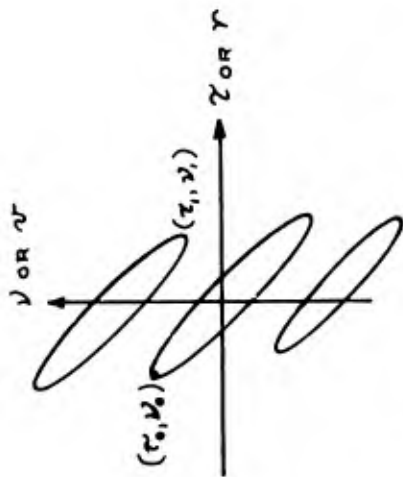
and the filters $H(\omega)$, $H_1(\omega)$ and $H_2(\omega)$ are used to obtain the appropriate restrictions. Equations (6.16) and (6.17) provide the essential result, that is, the spectrum of $\phi_o(\tau)$ expressed in terms of the spectra of $\phi_{o1}(\tau)$ and $\phi_{o2}(\tau)$. To find the equivalent operation in the τ -domain, (6.16) is transformed. The result is equation (4.10).

6.4 Coherent Frequency-Jump Burst Waveforms for TRADEX

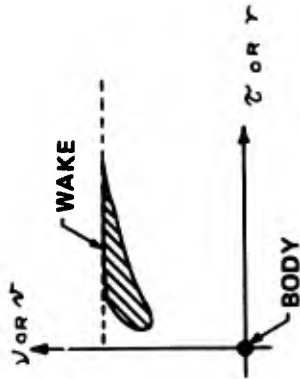
The properties of several coherent pulse trains are calculated using the results in Sections 3.4 and 3.5. The parameters apply to the TRADEX system. The results are expressed in meters and km/sec using the transformations (2.10a) and (2.10b). Results are presented in Table 6.1.

In particular, the coordinates of extreme nulls for the main lobe and first ambiguous lobe are of importance in determining possible ambiguous responses for reentry targets. Assuming that one wishes to resolve scattering regions on the body itself, one would adjust the doppler-parameter to the body velocity. Referring to Table 6.1, with the body at a zero doppler-offset ($\nu = 0$), one finds that, with waveform 1, the wake (typically at velocities of 5 to 7 km/sec with respect to the body) would not be observed (since there is no response at all for velocities between ν_0 and ν_f if $\nu_0 < \nu_f$). For waveforms 3 and 4, however, the return from the wake through the first ambiguous lobe may interfere with the body return. This might be avoided, at some sacrifice in the amplitude of the body return, by "detuning" the processing of a doppler-shift which is somewhat less than that of the body.

Constant-velocity profiles of waveforms 1 and 3 are given in Figures 6.5 and 6.6.



a) AMBIGUITY FUNCTION



b) R/V & WAKE SCATTERING FUNCTION
(PROCESSING TUNED TO BODY VELOCITY)

Figure 6.4 INTERPRETATION OF QUANTITIES IN TABLE 6.1

Table 6.1 PROPERTIES OF CANDIDATE WAVEFORMS FOR TRADEX

WAVEFORM	PULSE BANDWIDTH B MHz	PULSE DURATION T μ sec	PULSE SPACING Δf MHz	PULSE SPACING Δt μ sec	NUMBER OF PULSES N	BURST DURATION μ sec	COORDINATES OF EXTREMES FOR MAIN LOBE AND FIRST AMBIGUITY (SEE FIGURE 6.4)				AMBIGUOUS RANGE INTERVAL γ _a (meters)
							γ ₀ (M)	ν ₀ km/sec	γ ₁ (M)	ν ₁ km/sec	
1	60	3	9.6	4	19	75	- 5.7	4.5	3.6	9.7	530
2	60	3	9.6	5	19	93	- 5.5	3.5	3.9	7.5	680
3	60	3	19.2	4	10	39	- 6.6	10.5	4.1	5.9	460
4	30	1.5	9.6	4	22	85.5	-11.4	9.1	9.2	5.1	530

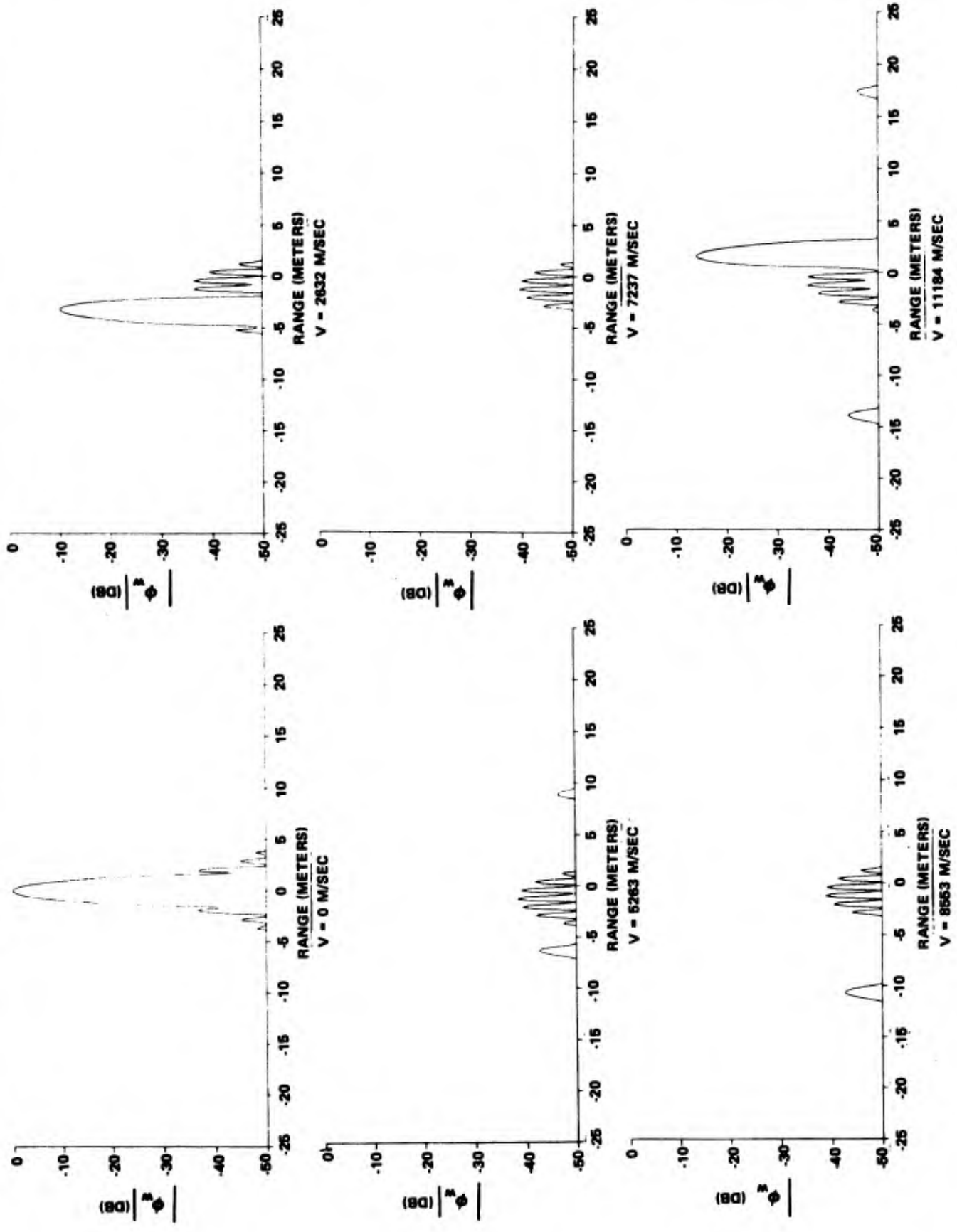


Figure 6.5 CONSTANT-VELOCITY PROFILES FOR WAVEFORM 1
 ($\Delta_f = 9.6$ MHz, $\Delta \epsilon = 4 \mu\text{SEC}$)

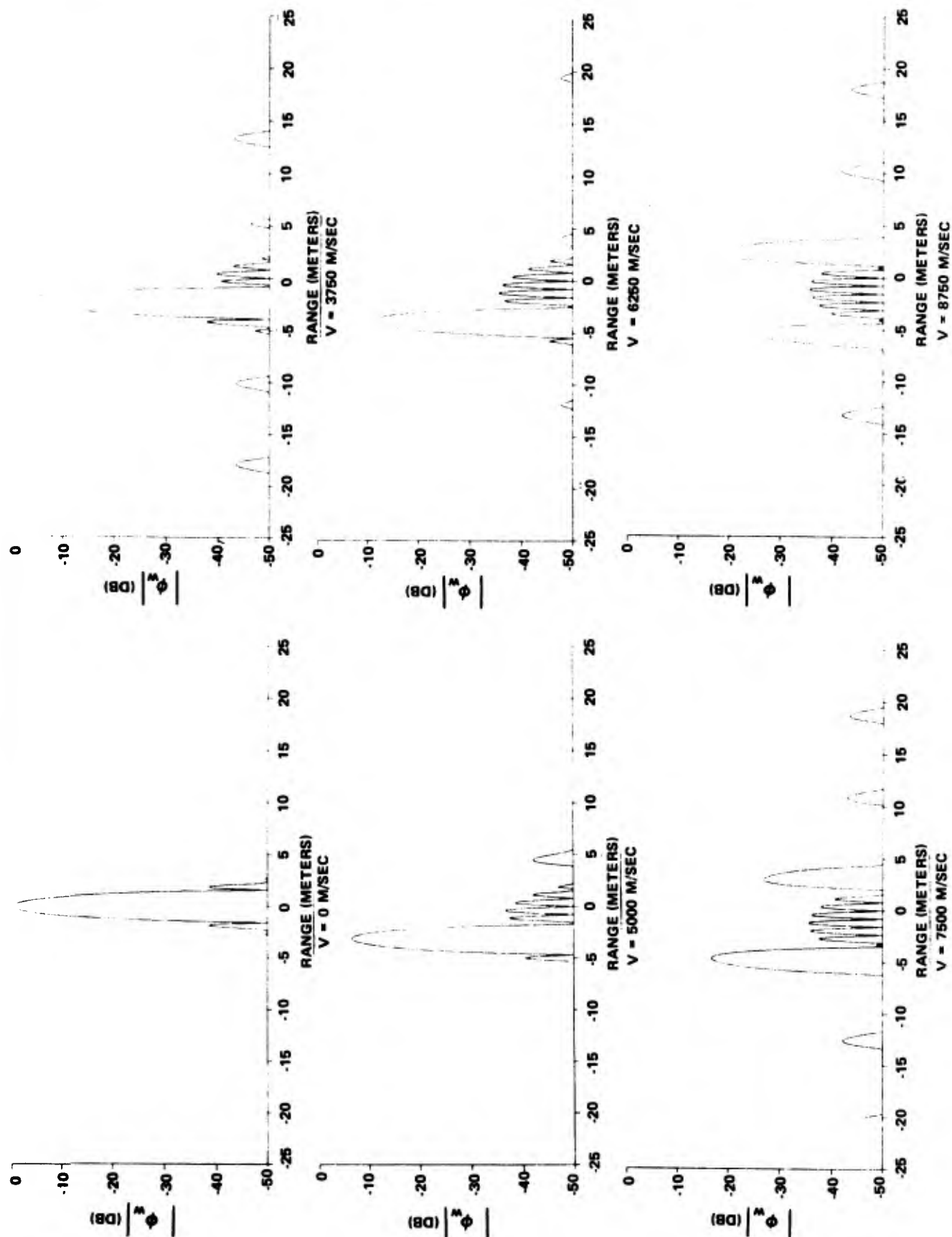


Figure 6.6 CONSTANT-VELOCITY PROFILES FOR WAVEFORM 3
 $(\Delta_f = 19.2 \text{ MHz}, \Delta_t = 4 \mu\text{SEC})$